Int. J. Heat Mass Transfer. Vol. 30, No. 10, pp. 2031–2044, 1987
Printed in Great Britain

0017–9310/87 $3.00 + 0.00

A complete model of the drying curve for porous bodies—experimental and theoretical studies

N. SCHADLER and W. KAST
Technische Hochschule Darmstadt, Federal Republic of Germany

(*Received* 15 *April* 1986 *and in revised form* 11 *February* 1987)

Abstract—Non-hygroscopic, capillary porous bodies, saturated with liquids were dried in an experimental device. By systematically varying the drying agent, the liquids and the differently structured samples, a wide range of drying rate curves were found experimentally and evaluated. The basic equation for the model of the constant-rate drying period refers—according to Krischer—to capillary liquid transportation only. The liquid-diffusion coefficient dependent on moisture content is calculated on the basis of the model considerations of Rumpf. For the falling-rate period the well-known receding drying front model is modified with regard to the capillary liquid movement.

1. INTRODUCTION

THE DRYING behaviour of non-hygroscopic, capillary porous materials has been investigated in many publications. This can be explained firstly by the particularity of drying processes and secondly by the fact that test results can rarely be transferred to other similar structured bodies.

However, most theoretical drying models only describe the respective experimental results. In most cases it will be very difficult, to apply that very model to other test results. Sometimes the problem can be solved by modification of parameters or even by the introduction of other characteristic factors.

This paper intends to investigate the most important influences on the drying rate. A simple model has been modified in such a way that the calculation of drying rates for non-hygroscopic materials is possible. Hence, the following tasks can be formulated:

(a) the calculation of the constant-rate period with critical moisture content and;

(b) the calculation of the falling-rate period with small calculation effort using only a reduced number of characteristic units.

The experimental equipment was designed to register all necessary data automatically. The investigations were limited to convective drying with the influence of radiation from the surrounding walls.

Table 1. Liquids

Water	WAT	H_2O
Ethylalcohol	ETH	C_2H_6O
Benzene	BEN	C_6H_6
n-Hexane	HEX	C_6H_{14}
Methanol	MET	CH_4O
Propanol (1)	PRO	C_3H_8O
Tetrachloromethane	TET	CCl_4
Toluene	TOL	C_7H_8

The cylindrical samples (diameter 23 mm) were blown across by the air stream. The diameter for spherical samples was 20 mm. The different liquids used are listed in Table 1. The air velocity was varied between 0.15 and 0.35 m s^{-1}, and the air temperature between 30 and 70°C. The humidity Φ of the drying air was reduced to zero.

2. DESCRIPTION OF EXPERIMENTS

2.1. *Test equipment*

The experimental equipment is shown in Fig. 1. Jokisch's apparatus [1] was modified with further instruments being added.

The air velocity can be varied by movable membrane pumps (1) and measured with a calibrated rotameter (7). The humidity of drying air is reduced to ≈ 0 g H_2O/kg air using a cooling trap (3, 4) and two drying columns (drying silica gel column (5) and drying P_2O_5 column (6)). The air temperature is controlled by a thermocouple which automatically operates the electric heating. Air and test section temperatures are the same.

All temperatures are determined with NiCr–Ni thermocouples; the thermoelectric voltage of which is transferred either to temperature controllers (16, 17) or to a data transfer unit (22) or to the printer (21). The surface temperature of the sample is measured by an infra-red thermometer (19), which is based on the measuring of radiation differences. The infra-red thermometer had a temperature range of -25 to 75°C and a spectroscopic sensitivity of 8 to 14 μm. The reaction time is 1 s and the absolute accuracy is ± 0.75 K. Using further thermocouples, it can be increased to a relative accuracy of ± 0.2 K. The signal of the infra-red thermometer (19) is adapted to guide-arrangement (20) and the d.c. signal (0–1000 mV) is passed on to the data transfer unit (22). The advantage of the infra-red thermometer is that the emissivity ε of the sample can be divided in 1/100 steps between 0.10 and 1.00.

NOMENCLATURE

A	area [m^2]
a	thermal diffusivity [$m^2 s^{-1}$]
c_p	specific heat capacity at constant pressure [$J kg^{-1} K^{-1}$]
D	diffusion coefficient [$m^2 s^{-1}$]
$\bar{d}$	mean diameter [m]
e	extend [m]
Δh_v	specific latent heat of vaporization [$J kg^{-1}$]
K	function, equation (3) [—]
l	length [m]
M	molar mass [$kg kmol^{-1}$]
m	mass [kg]
$\dot{m}$	mass flux density [$kg m^{-2} s^{-1}$]
p	pressure [$N m^{-2}$]
$\dot{q}$	heat flux density [$W m^{-2}$]
$\mathbb{R}$	universal gas constant, 8.314 $J mol^{-1} K^{-1}$
R, r	radius [m]
S	liquid saturation, ψ_l/ψ [—]
T	thermodynamic temperature [K]
t	time [s]
u	velocity [$m s^{-1}$]
w	water content, $\psi_l(\rho_l/\rho_{so}) = (\rho_l/\rho_{so})\psi S$ [$kg kg^{-1}$].

Greek symbols

α	heat transfer coefficient [$W m^{-2} K^{-1}$]
β	mass transfer coefficient [$m s^{-1}$]
Δ	difference [—]
$1/\Delta$	resistance by mass transfer [$s m^{-1}$]
η	dynamic viscosity [$kg m^{-1} s^{-1}$]
η_n	normalized moisture content [—]
θ	Celsius temperature [°C]
κ	liquid diffusion coefficient [$m^2 s^{-1}$]
λ	thermal conductivity [$W m^{-1} K^{-1}$]
$1/\Lambda$	resistance by heat transfer [$m^2 K W^{-1}$]
μ	resistance coefficient [—]
$\mu_{l(\kappa)}$	liquid resistance coefficient [—]
ν	kinematic viscosity [$m^2 s^{-1}$]
ρ	density [$kg m^{-3}$]
σ	surface tension [$N m^{-1}$]
ψ	void fraction [—].

Subscripts

a	air
C	convection
cap	capillary
cr	critical
d	deep
dry	dry
I	constant-rate period
l	liquid
lam	laminar
m	mean
R	radiation
r	relative
s	surface
so	solid
SV	volume equal to a sphere
v	vapour
0	initial.

Superscripts

''	saturated
*	correction.

Dimensionless parameters

Ca	capillary number, We/Re
K_r	for equation (6) $[(S-S_{min})/(1-S_{min})]^{3.5}$.

For continuous weight measurement the sample to be dried is suspended on an electronic balance (13) (accuracy 0.1 mg). The digital signal of the balance is transformed by D/A change (14) and then passed to the data transfer unit.

The data needed for the drying rate can be transferred from the data transfer unit (22) to a teletype and a puncher. At the beginning of the tests, it is possible to indicate all important data (e.g. experimental number, dimension size, liquid, etc.) on the teletype.

2.2. *Materials*

The investigated materials are non-hygroscopic, capillary porous bodies which are solvent resistent. Sintered bodies of crushed glass with different granular size and ceramic filterstones were used. Furthermore, the materials had to be different in pore size, porosity, and mean capillary radius. The materials and their characteristic data are listed in Table 2. The density and porosity data are mean values measured in vacuum wetted samples. The diffusion-resistance coefficient μ_{dry} is determined in accordance to DIN 52615. The mean capillary radius is taken from data sheets of deliverers. In order to check these data the pore size distributions of the fine capillary materials have been investigated. The experimental results of the pore size distributions are shown in Fig. 2, in comparison to the data by Sommer [2] for pumice concrete, clay brick, and a glass spheres column. According to Zehner and Schlünder [3] the thermal conductivity λ_{dry} of the porous material can be derived from the thermal conductivity λ_{so} of the solid material.

2.3. *Experimental procedure*

The interfacial area A for heat and mass transfer is determined by the dimensions of the samples. The drying rate is found by the weight loss Δm_i in the time

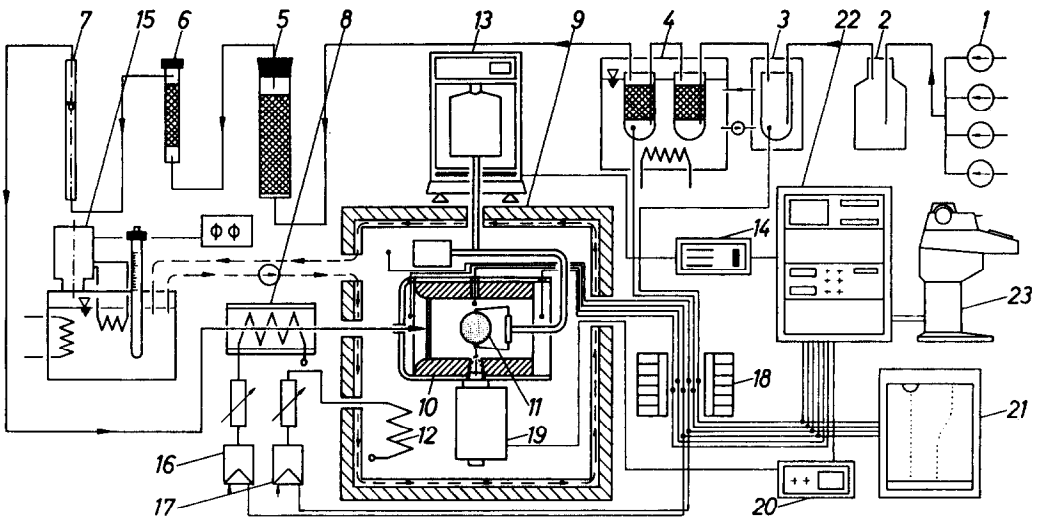

FIG. 1. Schematic diagram of experimental equipment.

Δt. For the graph the function $\dot{m} = f(w_m)$ is chosen, w_m being the mean moisture content. This leads to the following equation:

$$\dot{m} = \frac{1}{A}\frac{\Delta m_l}{\Delta t}$$

and

$$w_m = \frac{m_l}{m_{dry}}.$$

Two sequential pairs of values substitute the differential quotient by the difference quotient.

The same method of calculation was used to determine the graph $\theta_s = f(w_m)$. The measurement of the surface temperature with an infra-red thermometer is only possible if the emissivity ε of the sample is known. The influence of the surrounding temperature has to be considered.

3. MATHEMATICAL MODELLING

3.1. *General remarks*

For the calculation of drying rates, it is necessary to describe the physical facts sufficiently correct. For that purpose, the drying of non-hygroscopic materials is described with the following two different models.

(a) The constant-rate period is predominant as long as the surface of the porous body is sufficiently

Table 2. Characteristics of the investigated materials

Sample	Density, ρ [kg m^{-3}]	Porosity, ψ [%]	Diff. resistance coefficient, μ_{dry} [−]	Mean capillary radius, $r_{m,cap}$ [μm]	Thermal conductivity of solid material, λ_{so} [W m^{-1} K^{-1}]
Crushed glass P1	1580	29	3.2	37	1.2
Crushed glass P4	1230	44	2.3	3.4 (4.7)†	1.2
Crushed glass P5	1720	23	5.5	0.44 (0.47)†	1.2
Filterstone T3	1250	43	3.5	50	2.5
Filterstone S3	1500	35	3.8	45	4.5
Filterstone A1	1340	43	3.0	12.5	4.5
Filterstone G8	1470	51	2.8	0.9 (0.88)†	1.5

† Mean capillary radii in parentheses from pore size distribution by $\psi_l/\psi = 50\%$.

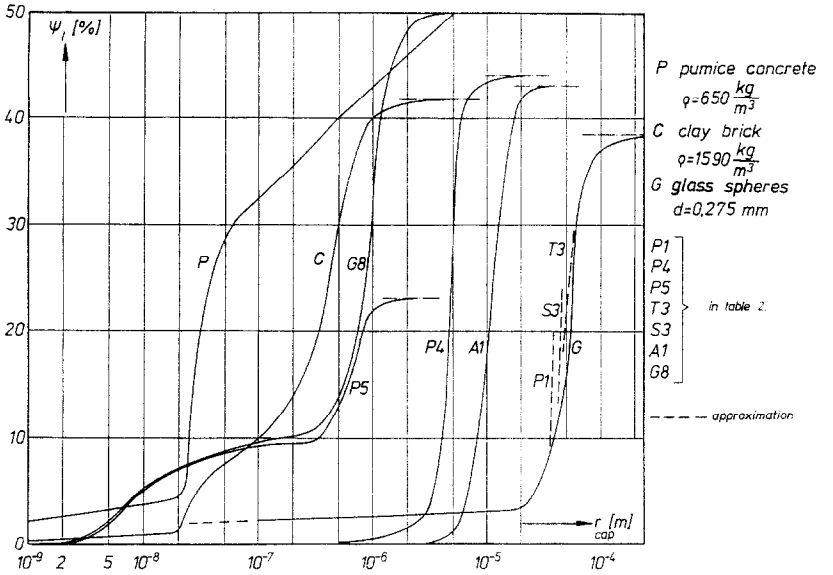

FIG. 2. Cumulative pore size distribution.

wetted due to capillary moisture movement. If the drying material is structured like a spheres packing, in both cases the analogous mathematical interrelationship for liquid movement can be applied. The calculation of the moisture movement inside the porous body follows a proposal made in ref. [4]. However, the determination of the liquid diffusion coefficient κ, depending on moisture content, is based on the capillary pressure function $p_{cap} = f(\psi_l)$ of an ideal spheres packing as proposed by Rumpf and Schubert. According to Charé [5] the model has been applied to the drying of agglomerates.

(b) For the falling-rate period, the evaporation front migrates into the porous body. Therefore, the capillary liquid movement is reduced and the description of physical facts needs a second model. Again according to ref. [4], the moisture movement can be described with the model of a receding drying front. This model is based on the assumption, that the evaporating liquid diffuses from the drying front through dry material layers to the surface and then into the air. Many authors used this model, see e.g. refs. [6–10].

It is the aim of this study to explain and extend both models in a way, that a predetermination of the drying rate is possible.

3.2. *Constant-rate period with critical moisture content*

The capillary liquid movement analogous to the second Fickian law can be described as

$$\frac{\partial w}{\partial t} = \nabla(\kappa \nabla w) \tag{1}$$

where w is the local moisture content (kg liquid/kg dry material) and κ the liquid diffusion coefficient depending on moisture content.

Krischer treated the porous system as a bundle of interconnected capillary tubes with increasing radii from r_{min} to r_{max}. Using the function of pore size distribution $\psi_l = f(r_{cap})$ the following equation can be derived:

$$\kappa = \frac{\sigma}{4\eta} \frac{\int_{r_{min}}^{r_z} r^2 \frac{d\psi_l}{dr} dr}{r^2 \frac{d\psi_l}{dr}\Big|_{r_z}} \tag{2}$$

where r_z is the radius of a capillary still filled with liquid in the respective cross-section. The additional resistance of fluid flow by detours, narrow and extended capillary paths was regarded by Sommer [2] introducing a factor $\mu_{l\kappa}$. This factor increases with decreasing moisture content, the sequence of filled and empty pores being the reason for the reduced capillary liquid movement.

Another method to define the coefficient of capillary liquid movement is based on the considerations of Rumpf. Capillary moisture movement can be interpreted as liquid flow through a porous medium caused by a suction potential. So, the flow rate can be expressed by Darcy's law

$$\dot{m}_l = A \rho_l K \frac{dp_{cap}}{dl}. \tag{3}$$

The capillary pressure p_{cap} is the suction potential and $K = K_0 K_r$ is the permeability depending on moisture content. Assuming the simple case that the porous system is still completely filled with liquid ($\psi_l = \psi$) and no dehydration occurs the capillary pressure p_{cap}

causes a flow through the system ($\rightarrow K = K_0$). According to Krischer

$$\dot{m}_l = A\psi \frac{b_{lam}}{\mu_l} \frac{\Delta p}{l} \tag{4}$$

where

$$b_{lam} = \frac{d_{equ}^2}{32v}$$

is a mobility factor (Hagen–Poiseuille)

$$d_{equ} = \bar{d}_{cap}$$

defines the equivalent capillary diameter and μ_l (= 2.3 after ref. [4]) is the factor for the path length. From equations (3) and (4) it follows that

$$K_0 = \frac{\psi}{\rho_l} \frac{b_{lam}}{\mu_l} = \frac{\psi^3}{(1-\psi)^2} \frac{d_{SV}^2}{165\eta}. \tag{5}$$

For the calculation of $\bar{d}_{cap}$ the sphere diameter d is needed. This diameter can be defined by d_{SV} (diameter of a sphere with the same volume as a single particle).

Brutsaert proposed an exponential function for the relative permeability and Schubert [13] found a geometrical function for the relative capillary pressure depending on the 'bridge volume' (liquid interlinking the particles). Finally Charé [5] found an approximate function for the differentiation of the relative capillary pressure to 'bridge volume'. Therefore, the liquid diffusion coefficient can be defined approximately by

$$\kappa(S) = \frac{\sigma d_{SV}}{\eta} K_r \frac{\psi^3}{165(1-\psi)^2} \times 0.325 \left[\frac{\psi^2}{(1-\psi)\pi}\right]^{-0.63} S^{-1.63}. \tag{6}$$

In equation (6) there are two free parameters for each liquid.

(a) Mean diameter d_{SV} of the particles, determined statistically.

(b) Minimum saturation degree S_{min}. By model calculation of equal spheres packings according to Schubert [13] an approximate value can be found.

With the liquid diffusion coefficient from equation (6), the transport equation (1) can be solved numerically regarding the geometry of the sample. The differential equation (1) has two boundary conditions and one initial condition:

for

$$t = 0: \quad w = w_0$$

$$t \geqslant 0: \quad \left.\frac{\partial w}{\partial r}\right|_{r=0} = 0$$

and

$$0 < t \leqslant t_{cr}: \quad \dot{m}_l + \kappa(w)\rho \left.\frac{\partial w}{\partial r}\right|_{r=R} = 0.$$

The drying rate $\dot{m}_l$ (constant-rate period) is determined by heat and mass transfer.

The calculated moisture gradient in the porous body is small within the constant-rate period as shown schematically in Fig. 3. The end of the constant-rate period is determined by a large moisture gradient at the sample surface (critical moisture content) [5].

3.3. *Falling-rate period*

The heat and mass transfer equations for the receding drying front will be explained with the aid of Fig. 4. It is assumed in this model that the drying of the sample will be constant across the material and so that at the beginning of the falling-rate period the mean measurable critical moisture content $w_{m,cr}$ is constant as well. The calculation of the constant-rate period confirms this assumption approximately (Fig. 3). Reaching the critical moisture content, the evaporation front migrates into the porous body separating the moist part with $w = w_{m,cr}$ from the dry part with $w = 0$. The receding drying front evaporation takes place at the respective temperature θ_d. Moisture is transported to the surface through the dry body layers by vapour diffusion.

The heat and mass transfer (convection and radiation) in the falling-rate period can be described by

$$\dot{q} = \frac{\Delta h_v(\theta_d)}{c_p} \frac{1}{1/\alpha + 1/\Lambda} \ln\left[1 + \frac{c_p}{\Delta h_v(\theta_d)}(\theta_a - \theta_d)\right],$$

$$\alpha = \alpha_C + \alpha_R \tag{7}$$

$$\dot{m} = \frac{pM_l}{\mathbb{R}T} \frac{1}{1/\beta + 1/\Delta} \ln\left[1 + \frac{p''_{vd} + p_{va}}{p - p''_{vd}}\right] \tag{8}$$

$$\dot{q} = \dot{m} \cdot \Delta h_v(\theta_d). \tag{9}$$

$1/\Lambda$ and $1/\Delta$ are the heat resistance and mass transport resistance inside the body. They depend on the

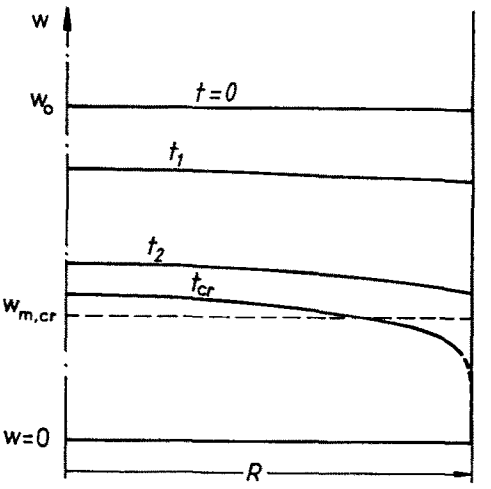

FIG. 3. Moisture content in constant-rate period schematically.

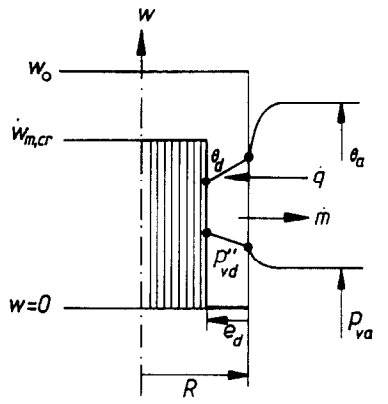

FIG. 4. Heat and mass transfer in falling-rate period.

geometric shape:

cylinder

$$\frac{1}{\Lambda}=\frac{R}{\lambda_{dry}}\ln\frac{1}{1-e_d/R};\quad \frac{1}{\Delta}=\frac{\mu_{dry}R}{D}\ln\frac{1}{1-e_d/R}; \tag{10}$$

sphere

$$\frac{1}{\Lambda}=\frac{R}{\lambda_{dry}}\frac{e_d/R}{1-e_d/R};\quad \frac{1}{\Delta}=\frac{\mu_{dry}R}{D}\frac{e_d/R}{1-e_d/R}. \tag{11}$$

For an *ideal* drying medium the respective position of the drying front e_d/R is a function of dimensionless moisture content $\eta_n = w/w_{m,cr}$. The following coupling equations are valid:

$$1-\frac{e_d}{R}=\sqrt{\eta_n}\quad \text{for cylinders} \tag{12}$$

and

$$1-\frac{e_d}{R}=\eta_n^{1/3}\quad \text{for spheres.} \tag{13}$$

With the help of equations (10) and (11) the so-called 'moisture functions' can be described:

for cylinders

$$f(\eta_n)=\ln\frac{1}{\sqrt{\eta_n}} \tag{14}$$

and for a sphere

$$f(\eta_n)=\frac{1}{\eta_n^{1/3}}-1. \tag{15}$$

According to the results given by Schadler [14], for *real* drying media the evaporation front migrates slower into the porous body, i.e. the capillary liquid movement cannot be neglected as compared to the vapour diffusion. It is obvious that the moisture function needs a correction. The position of the evaporation front is influenced by the capillary liquid movement. Hence

$$f^*(\eta_n)=f(\eta_n)\frac{\mu_{lk}(\eta_n)}{\mu_{lk}(\eta_n\to 0)} \tag{16}$$

with

$$\mu_{lk}(\eta_n)=\mu_{lk}(\eta_n\to 0)+[1-\mu_{lk}(\eta_n\to 0)]\eta_n. \tag{17}$$

The liquid movement beyond the evaporation front can be regarded by the introduction of the resistance coefficient for liquid transport $\mu_{lk}(\eta_n)$. For model considerations it is assumed that between the evaporation front and the surface of the porous body only vapour diffusion can be important and therefore in this range μ_{lk} is infinity. With an analogous calculation for the diffusion resistance coefficient μ_{dry}, Jaeschke [12] could estimate the capillary liquid diffusion.

The boundary analysis of $\mu_{lk}(\eta_n)/\mu_{lk}(\eta_n\to 0)$ for $\mu_{lk}(\eta=0)=\infty$ leads to $1-\eta_n$. Hence, the corrected moisture function is given by

$$f^*(\eta_n)=f(\eta_n)(1-\eta_n). \tag{18}$$

With $f^*(\eta_n)$ the probable evaporation front e_d^* can be calculated, if the implicitly included factor e_d in equation (14) or (15) is replaced by the factor e_d^*.

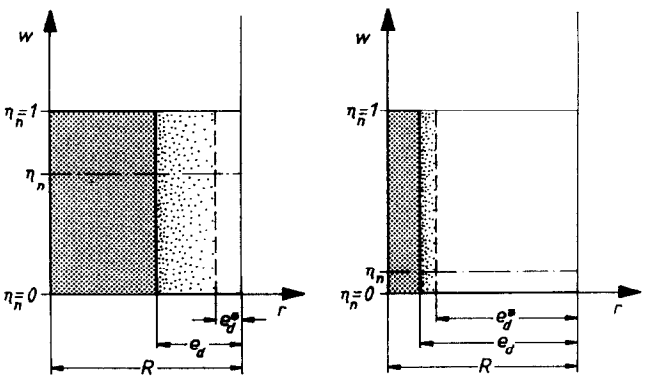

FIG. 5. Receding drying-front model with correction.

The dimensionless moisture content for $\eta_n < 1$ and $\eta_n \ll 1$ is plotted against the sample radius in Figs. 5(a) and (b), respectively. It follows, that by the correction of the moisture function the position e_d^* is marked where capillary liquid movement is zero. The moisture functions f and f^* are compared for well-known standard shapes such as a cylinder, a sphere, and a slab in Fig. 6.

Schlünder *et al.* tried to correct the moisture function. They found a correction by close adaption to test results. Moreover, Haertling [8] found a correction of the moisture function independent of the shape.

For the temperature θ_d (drying-front temperature) with equations (7)–(9) it follows that

$$\theta_a - \theta_d = \frac{\Delta h_v(\theta_d)}{c_p} \times [(1+B_T)^{\gamma^*[(1+Bi\,f^*(\eta_n))/(1+Bi'\,f^*(\eta_n))]} - 1] \quad (19)$$

with

$$B_T = \frac{p''_{vd} - p_{va}}{p - p''_{vd}}$$

$$Bi = \frac{(\alpha_C + \alpha_R)R}{\lambda_{dry}} \quad \text{Biot number for heat transfer}$$

$$Bi' = \frac{\beta \mu_{dry} R}{D} \quad \text{Biot number for mass transfer}$$

$$\gamma^* = \frac{c_p M_1}{c_p M}\left(\frac{a}{D}\right)^{2/3} \frac{\alpha_C}{\alpha_C + \alpha_R}.$$

Equation (19) is solved by iteration. So, the drying rate can be calculated with equation (8). The connected surface temperature in the falling-rate period is

$$\theta_s = \frac{\theta_a + \dfrac{\alpha_R}{\alpha_c}\theta_R + \dfrac{1}{\alpha_C(1/\Lambda)}\theta_d}{1 + \dfrac{\alpha_R}{\alpha_C} + \dfrac{1}{\alpha_C(1/\Lambda)}}. \quad (20)$$

4. RESULTS AND DISCUSSIONS

In Figs. 7–13 the drying rate is plotted against the mean moisture content. The symbols indicate the results of the analytical calculation. Only a few drying experiments are presented.

4.1. *Drying rates*

Heat and mass transfer coefficients have been determined using the measured drying rate and the surface temperature in the constant-rate period. The model calculation of the moisture diffusivity κ as presented by Charé [5] needs an equivalent particle diameter and a minimum degree of saturation. The investigated bodies are sintered consisting of unporous particles of specified granular diameter. The pore size of the samples is mainly defined by the grain size. In connection with pictures from an electron-scan microscope the following equivalent particle diameters resulted out of a collective of particles:

T3: $d_{SV} = 400\ \mu m$

P1: $d_{SV} = 350\ \mu m$

P4: $d_{SV} = 30\ \mu m$

P5: $d_{SV} = 10\ \mu m$.

An indication for $S_{min} = \psi_{l,min}/\psi$ can be found with the help of a model packing of equal spheres [13]. P-Samples are different in porosity, however, with

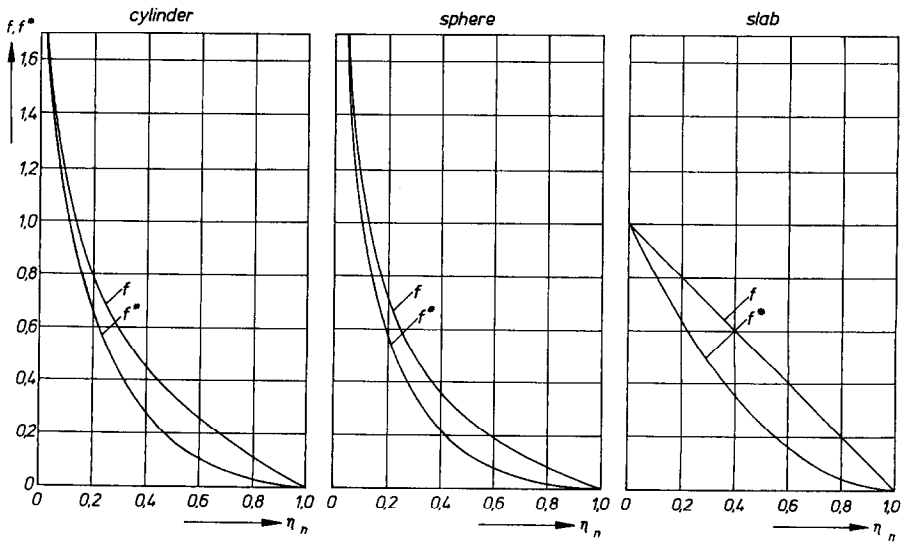

FIG. 6. Moisture function f, f^* as a function of normalized moisture content.

Symb.	No.	Sample	Liquid	Air θ [°C]	Air u [m/s]
○	33	P1	WAT	30.0	0.22
△	31	P1	MET	30.0	0.22
+	39	P1	BEN	30.0	0.22

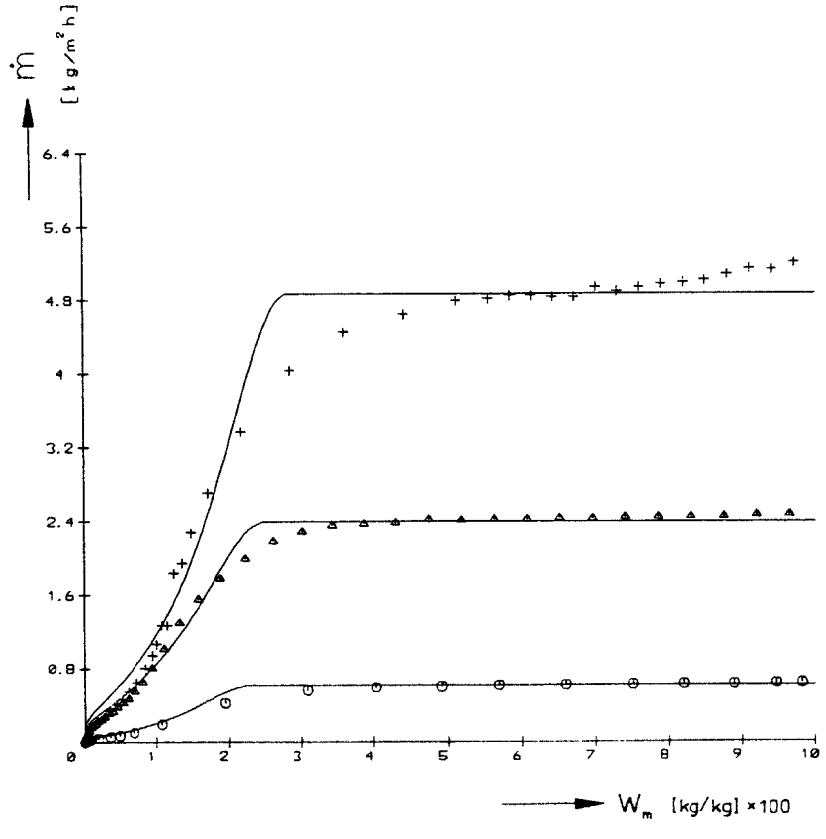

FIG. 7. Comparison of calculated and measured drying rate curves of crushed glass P1 cylinder.

Symb.	No.	Sample	Liquid	Air θ [°C]	Air u [m/s]
○	32	P4	WAT	30.0	0.21
△	30	P4	MET	30.0	0.21
+	38	P4	BEN	30.0	0.22

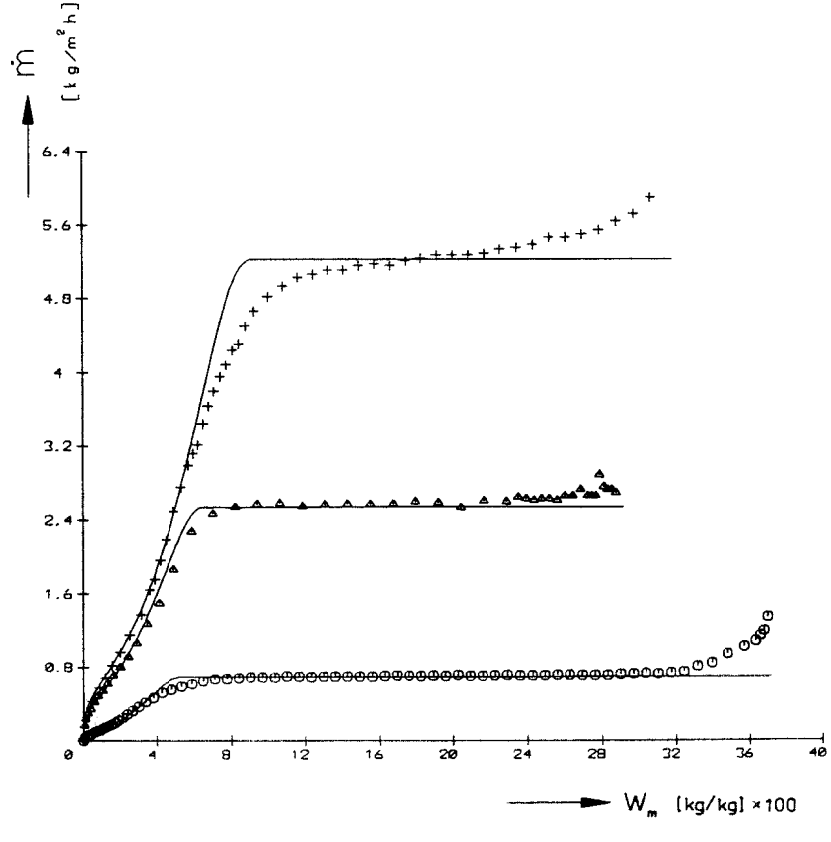

FIG. 8. Comparison of calculated and measured drying rate curves of crushed glass P4 cylinder.

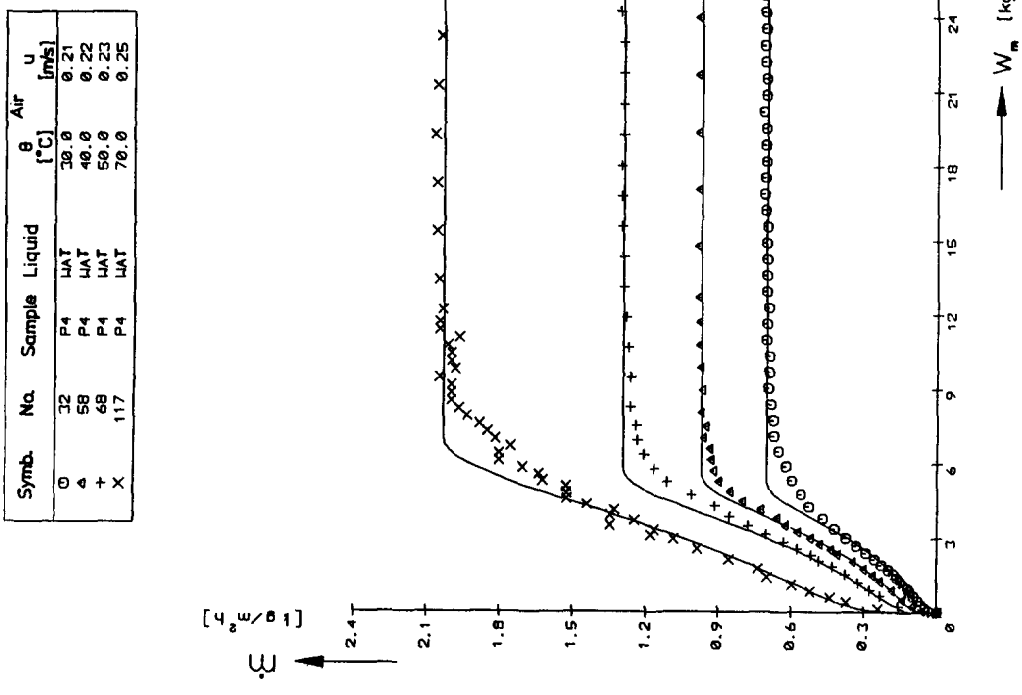

FIG. 9. Comparison of calculated and measured drying rate curves of crushed glass P4 cylinder for water.

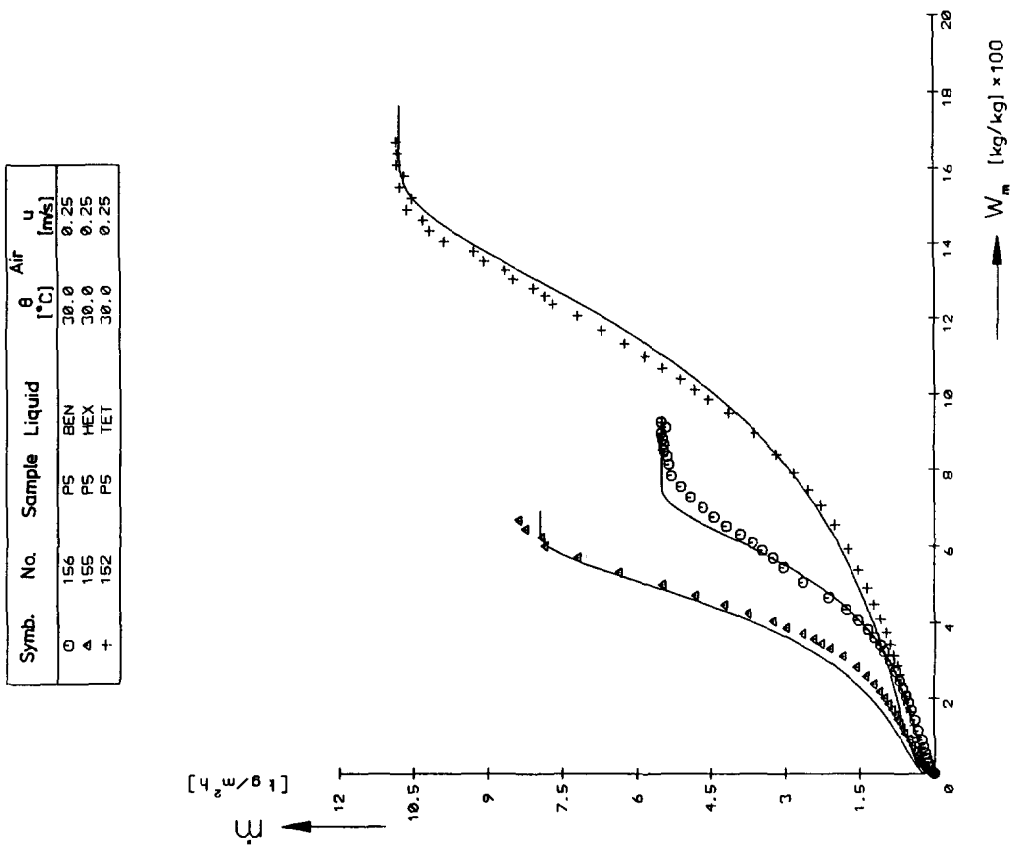

FIG. 10. Comparison of calculated and measured drying rate curves of crushed glass P5 cylinder.

Symb.	No.	Sample	Liquid	Air θ [°C]	Air u [m/s]
○	214	T3	WAT	30.0	0.22
△	220	T3	MET	30.0	0.22

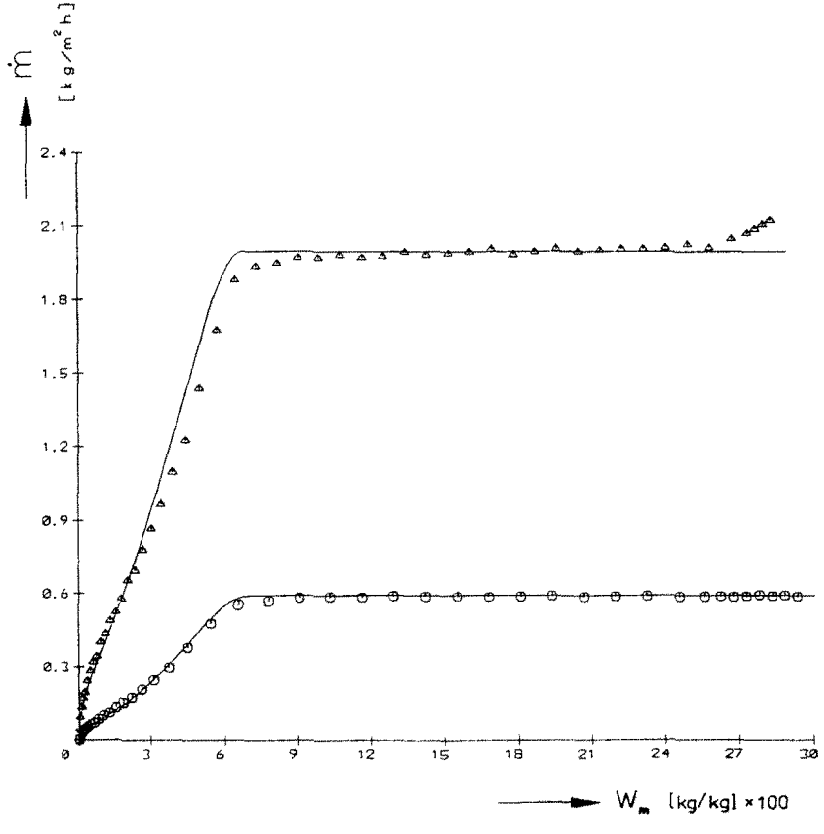

FIG. 11. Comparison of calculated and measured drying rate curves of filterstone T3 sphere.

Symb.	No.	Sample	Liquid	Air θ [°C]	Air u [m/s]
○	238	T3	BEN	30.0	0.22
△	256	T3	TET	30.0	0.22

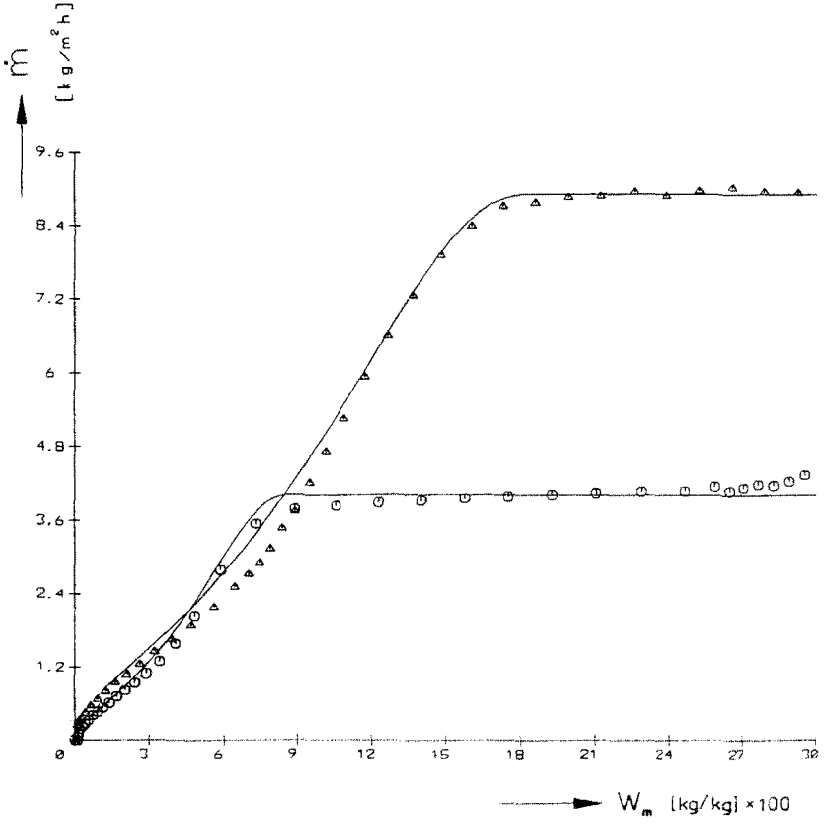

FIG. 12. Comparison of calculated and measured drying rate curves of filterstone T3 sphere.

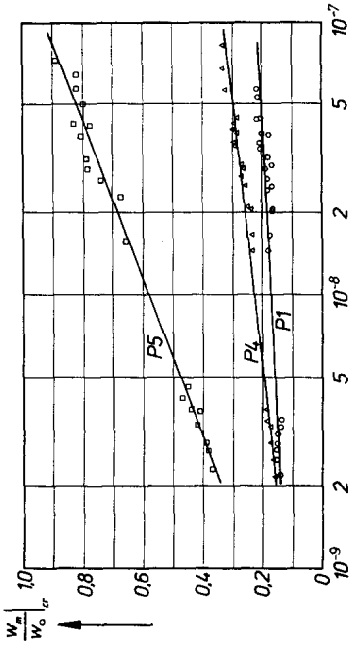

FIG. 14. Experimental results for normalized critical moisture content as a function of capillary number (crushed glasses).

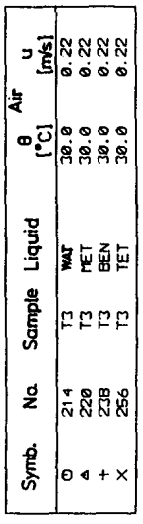

Symb.	No.	Sample	Liquid	θ Air [°C]	u [m/s]
○	214	T3	WAT	30.0	0.22
△	220	T3	MET	30.0	0.22
+	238	T3	BEN	30.0	0.22
×	256	T3	TET	30.0	0.22

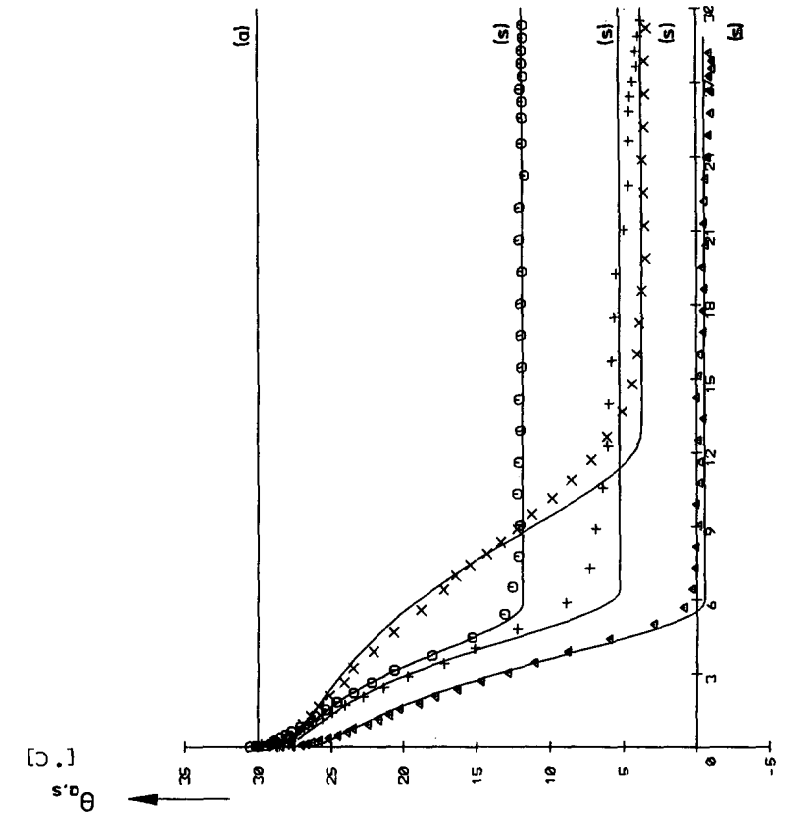

FIG. 13. Comparison of calculated and measured surface temperature of filterstone T3 sphere.

$S_{min} = 0.04$ a good agreement between measurements and calculations could be found. The minimum degree of saturation S_{min} for T3 samples is 0.14.

In Fig. 7 the liquids in cylindrical P1 samples are varied, while the other drying parameters such as air temperature and air velocity are kept nearly constant. It can be observed that the drying rates show a comparably low critical moisture content. With the analytical calculation for the constant-rate period the critical moisture content could be predicted with an accuracy of up to 15%, e.g. the experiment with benzene:

critical moisture content predicted, 3.2%

critical moisture content measured, 2.8%.

For this and the following experiments it can be demonstrated, that the present analytical model for the falling-rate period shows no sharp critical point at the end of the constant-rate period. Obviously the new model is better suited to describe the reality in that range. The analytical results for the falling-rate period show a sufficient agreement between predicted and measured drying rates. For all experiments with P1 samples the receding drying front model is calculated with the same diffusion resistance coefficient $\mu_{dry} = 3.2$.

In Fig. 8 the calculated and measured results of cylindrical P4 samples are compared. While the critical moisture content within P1 samples had only a small range of 2–3% comparable P4 samples show moisture contents of 5–9%. The model is able to describe the falling-rate period. The diffusion-resistance coefficient for all calculations is 2.3.

The applicability of both models for higher air temperatures was proven. Experiment and calculation are compared in Fig. 9. The specific data surface tension σ and viscosity η of the liquids are dependent on the temperature and clearly influence the critical moisture content. The analytical results describe this behaviour correctly.

In Fig. 10 the calculated and measured results of cylindrical P5 samples are compared. These show the lowest porosity (23%) among the crushed glass bodies. Therefore, the constant-rate period can only just be reached for some liquids (e.g. No. 156 benzene or No. 152 tetrachloromethane).

For another case the constant-rate period could not be observed clearly (No. 155 hexane) due to a high temperature at the beginning of the test. The model is able to predict the critical moisture content with an accuracy of 10%. The function f^*, allows the calculation of the drying rate within the falling-rate period and regards the capillary liquid transfer still available after critical moisture content sufficiently. The diffusion-resistance coefficient μ_{dry} found according to DIN 52615 equals 5.5. This result is confirmed by agreement between experiment and calculation also at the end of the drying rate curve.

For T3 samples a comparison of the predicted and experimental values is shown in Figs. 11 and 12. Contrary to the P samples, now the calculated critical moisture contents agree with experimental values. The model calculation of the falling-rate period with $\mu_{dry} = 3.5$ describes the drying rate for all liquids very well.

4.2. *Surface temperature*

The surface temperatures for spherical T3 samples are presented in Fig. 13. The symbols represent experimental data from an infra-red thermometer, while the full lines indicate the results of equation (20). The critical moisture content within the drying rate curve and the surface-temperature curve correspond only for experiments with water, for other liquids, the critical moisture contents are adapted to temperature curves. The critical moisture content within the temperature curves moves to smaller moisture contents as compared to the drying rate curves. It can be assumed, that the physical reason for this is the decrease of the drying rate due to reduced liquid transfer. Moreover, the heating up of the moist body is slower. The thermal conductivity of the moist bodies is directly proportional to the thermal conductivity of fluids. It is four times higher for solvents than for water.

4.3. *Critical moisture content*

According to Krischer, the critical moisture curve can be derived from a simple model of two interconnected capillary tubes and leads to

$$[\dot{m}_l s]_{cr} = \frac{\sigma \rho_l}{\eta} \frac{D_{cap}}{1 - w_m/w_0} = g(w_m/w_0)$$

where D_{cap} is a capillary function, s is R for cylinders and spheres and w_0 is the initial moisture content, which is not constant for different liquid densities. The equation can be transformed to

$$\left.\frac{w_m}{w_0}\right|_{cr} = f(m_{Dl}\eta/\sigma\rho_l, s) = f(Ca, s)$$

with the dimensionless capillary number $Ca = We/Re$ [15]. A comparison between the ratio $w_m/w_0|_{cr}$ and the logarithm of the capillary number is given by Figs. 14 and 15. Although the single results stray, the linearity of the function can be well recognized. With respect to the pore size of the different drying samples it can be summarized that for smaller capillaries and less porosity, the curve (in Figs. 14 and 15) is steeper and $w_m/w_0|_{cr}$ is larger. For very small pore size distributions the critical moisture content curves are not as steep, i.e. the critical moisture contents are less dependent on the capillary number Ca.

5. CONCLUSIONS

In this paper the drying rate of non-hygroscopic, capillary porous bodies, saturated with liquids, are investigated. The materials used had known pore size and are comparable with model packings.

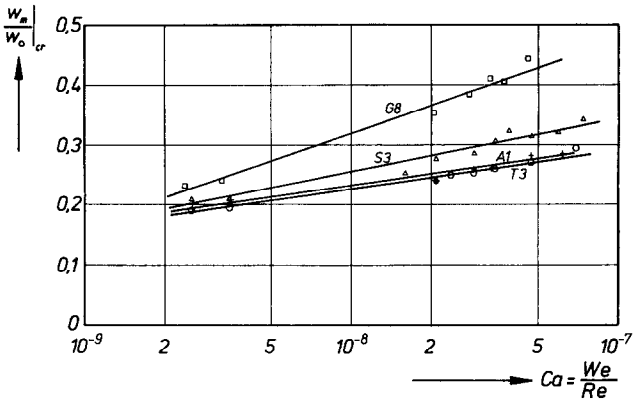

FIG. 15. Experimental results for normalized critical moisture content as a function of capillary number (filterstones).

In an extended test device, according to Jokisch, model bodies were dried. Sintered bodies of crushed glass and commercially available filterstones were used. The liquids selected allow the surface tension, viscosity and density to be modified. Due to the high evaporation rates of the liquids the drying rate can be varied in a wide range at low air velocity and at low air temperature. Using the model for the constant-rate period, it is possible to calculate the critical moisture content sufficiently accurately. The modified model for a receding drying front within the falling-rate period agrees well with experimental data and the results of other authors.

Acknowledgement—The author wishes to thank Prof. Dr.-Ing. W. Kast, Director of the Institut für Thermische Verfahrenstechnik und Heizungstechnik der Technischen Hochschule Darmstadt, for his guidance and the interest in this work.

REFERENCES

1. F. Jokisch, Über den Stofftransport im hygroskopischen Feuchtebereich kapillarporöser Stoffe am Beispiel des Wasserdampfes in technischen Adsorbentien, Dissertation, Technische Hochschule Darmstadt (1975).
2. E. Sommer, Beitrag zur Frage der kapillaren Flüssigkeitsbewegung in porigen Stoffen bei Be- und Entfeuchtungsvorgängen, Dissertation, Technische Hochschule Darmstadt (1971).
3. P. Zehner and E. U. Schlünder, Wärmeleitfähigkeit von Schüttungen bei mäßigen Temperaturen, *Chemie-Ingr-Tech.* **42,** 933 (1970).
4. O. Krischer and W. Kast, *Die wissenschaftlichen Grundlagen der Trocknungstechnik*, 3rd Edn. Springer, Berlin (1978).
5. I. Charé, Trocknung von Agglomeraten bei Anwesenheit auskristallisierender Stoffe. Festigkeit und Struktur der durch die auskristallisierten Stoffe verfestigten Granulate, Dissertation, Universität Karlsruhe (1976).
6. E. U. Schlünder, Fortschritte und Entwicklungstendenzen bei der Auslegung von Trocknern für vorgeformte Trocknungsgüter, *Chemie-Ingr-Tech.* **48,** 190 (1976).
7. G. Zabeschek, Experimentelle Bestimmung und analytische Beschreibung der Trocknungsgeschwindigkeit rieselfähiger, kapillarporöser Güter in der Wirbelschicht, Dissertation, Universität Karlsruhe (1977).
8. M. Haertling, Messung und Analyse von Trocknungsverlaufskurven als Grundlage zur Vorausberechnung von Trocknungsprozessen, Dissertation, Universität Karlsruhe (1978).
9. B. Keey, Vereinfachte Analyse der Trocknung kugelförmiger Güter, *Verfahrenstechnik* **13,** 933 (1979).
10. M. Suzuki, B. Keey and S. Maeda, *A.I.Ch.E. Symp. Ser. No. 163* **73,** 47 (1977).
11. R. Wyckoff and H. Botset, The flow of gas–liquid mixtures through inconsolidated sands, *Physics* **7,** 325 (1936).
12. L. Jaeschke, Mechanismus der Feuchtigkeitsbewegung bei der Trocknung von Gütern mit verkrustenden Oberflächen, *Chemie-Ingr-Tech.* **36,** 449 (1964).
13. H. Schubert, *Kapillarität in porösen Feststoffsystemen.* Springer, Berlin (1982).
14. N. Schadler, Untersuchungen zur Trocknung und Entwicklung eines Modells für die Berechnung des Trocknungsverlaufes kapillerporöser lösungsmittelfeuchter Körper, Dissertation, Technische Hochschule Darmstadt (1983).
15. A. Mersmann, Beispiele dimensionsloser Kennzahlen in der mechanischen Verfahrenstechnik, *Verfahrenstechnik* **5,** 23 (1971).

UN MODELE COMPLET POUR LA DESCRIPTION LES COURS DU SECHAGE DES CORPS CAPILLAIRES-POREUX—UNE ENQUETE EXPERIMENTALE ET THEORIQUE

Résumé—On a seché dans une installation d'essai des corps non-hygroscopiques capillaires-poreux et des dissolvants humides. En variant systematiquement les dessiccatif, les liquides et les différents échantillons structurés, on a pu trouver à l'échelle expérimental une large gamme des cours du séchage. L'équation fondamentale pour le modèle dans le premier segment du processus de séchage ne prend en considération—semblable à Krischer—que le transport des liquides capillaires. Le coefficient directeur d'humidité dépendant de l'humidité est defini sur la base de l'idée de Rumpf. Pour le deuxième segment de séchage le modèle de front d'évaporation déjà connu est modifié en tenant compte du transport de liquides capillaires.

EIN VOLLSTÄNDIGES MODELL ZUR BESCHREIBUNG DER TROCKENVERLAUFSKURVEN KAPILLARPORÖSER KÖRPER—EXPERIMENTELLE UND THEORETISCHE UNTERSUCHUNGEN

Zusammenfassung—In einer Versuchsanlage wurden nichthygroskopische, kapillarporöse, lösungsmittelfeuchte Körper getrocknet. Durch systematische Variation des Trockenmittels, der Flüssigkeiten und der unterschiedlich strukturierten Proben konnte eine breite Palette von Trockenverlaufskurven experimentell ermittelt werden. Die grundlegende Gleichung für das Modell im ersten Trocknungsabschnitt berücksichtigt—ähnlich wie Krischer—nur kapillaren Flüssigkeitstransport. Der feuchteabhängige Feuchteleitkoeffizient wird basierend auf Modellvorstellungen von Rumpf bestimmt. Für den zweiten Trocknungsabschnitt wird das bekannte Trockenspiegelmodell unter Beachtung des kapillaren Flüssigkeitstransportes modifiziert.

ПОЛНАЯ МОДЕЛЬ ПРОЦЕССА СУШКИ ДЛЯ ПОРИСТЫХ ТЕЛ. ЭКСПЕРИМЕНТАЛЬНОЕ И ТЕОРЕТИЧЕСКОЕ ИССЛЕДОВАНИЯ

Аннотация—В экспериментальной установке производилась сушка негигроскопических капиллярно-пористых тел. В широком диапазоне изменения параметров экспериментально определялись и оценивались кривые скорости сушки для различных образцов, заполненных жидкостями с различными физическими свойствами, при воздействии сушильного агента. Согласно Кришеру основное уравнение модели периода постоянной скорости сушки описывает только движение капиллярной жидкости. На основе модели Румпфа рассчитан коэффициент диффузии жидкости в зависимости от влагосодержания. Для периода падающей скорости сушки известная модель заглубления фронта испарения модифицирована для учета движения капиллярной жидкости.